Liu, W., Jin, M., Chen, C., You, R., and Chen, Q. 2016. "Implementation of a fast fluid dynamics model in OpenFOAM for simulating indoor airflow," *Numerical Heat Transfer, Part A: Applications,* 69(7): 748-762.

Implementation of a fast fluid dynamics model in OpenFOAM for simulating indoor airflow

Wei Liu[a, b], Mingang Jin[a], Chun Chen[a], Ruoyu You[a], Qingyan Chen[a*]
[a]School of Mechanical Engineering, Purdue University, West Lafayette, IN 47907, USA
[b]Tianjin Key Laboratory of Indoor Air Environmental Quality Control, School of Environmental Science and Engineering, Tianjin University, Tianjin 300072, China
*Corresponding email: yanchen@purdue.edu
Address: 585 Purdue Mall, West Lafayette, IN 47907-2088, U.S.A.
Phone: +1 (765) 496-7562
FAX: +1 (765) 494-0539

Abbreviated title: Implementation of a FFD model in OpenFOAM

Abstract

This study implemented FFD in OpenFOAM and used a local searching method that made the FFD solver applicable to unstructured meshes. Because the split scheme used in FFD is not conservative, this investigation developed a combined scheme that used split scheme for the continuity and momentum equations and iterative scheme for scalar equations. The combined scheme ensures conservation of the scalars. This investigation used two two-dimensional cases and one three-dimensional case, with experimental data, to test the FFD solver. The predicted results were similar with different types of meshes and numerical schemes and agreed in general with the experimental data.

Keywords: Structured mesh; unstructured mesh; split scheme; iterative scheme; semi-Lagrangian

Nomenclature

f_a, f_n	cell face index
F_i	body force in x_i direction
I_a, I_n	cell index
J	vector from X_a to X_d
N	number of grid cells
p	pressure
P	order of numerical scheme
r	grid refinement factor
S	source term
t	time
T	temperature
U	velocity
U_i, U_j	velocity components in x_i and x_j directions, respectively
U^n, U^{n+1}	velocity at previous and current time step, respectively

U^*, U^{**}	intermediate velocity
x, y	spatial coordinates
x_i, x_j	spatial coordinates in i and j direction, respectively
X_a, X_d	spatial coordinates of arrival point and departure point, respectively
X_{cr}^a, X_{cr}^n	spatial coordinates of crossover point
Γ	transport coefficient
v	kinetic viscosity
ρ	density
ϕ_1, ϕ_2	variables predicted with the use of structured and unstructured meshes, respectively
Φ	scalar in transport equation

1. Introduction

With the rapid development of computer technology, numerical simulations of indoor airflow have been widely used in design processes. These simulations have used multi-zone models, zonal models, and computational fluid dynamics (CFD), as summarized by Chen [1]. Multi-zone models can be very fast, but they only provide averaged characteristics of airflows and contaminant distributions within particular zones [2]. Significant errors may arise in large indoor spaces with stratified ventilation systems or strong jet momentums [3]. The use of zonal models can yield improvements over the "well-mixed" assumption of multi-zone models and can also provide fast simulations [4]. However, zonal models should be applied together with other models in regions with strong buoyancy or jet momentum. Thus, the accuracy of a zonal model depends on the user's ability to identify different flow characteristics in different regions. CFD simulation provides the most detailed information about distributions of air velocity, temperature, contaminant dispersion, etc. When it is used for indoor airflow simulations, CFD is also the most accurate approach, as it involves the fewest assumptions. CFD simulation is therefore the most popular method used today in design practice [1]. However, this method requires a powerful computer in order to handle a large number of grids for a large or complex indoor space, and the computing time can be very long [5]. A fast method is desired that can provide detailed indoor airflow information as does CFD and that is as efficient as are the nodal models.

Fast fluid dynamics (FFD), which solves the Navier-Stokes (NS) equations with a time-advancement scheme and a semi-Lagrangian (SL) scheme, seems to meet the above requirements. FFD has been widely applied to weather prediction and the study of atmospheric flows [6, 7, 8, 9]. Since the major development by Stam [10] in the area of computer games, FFD has been used for flow simulations. Zuo and Chen [11] applied FFD to fast two-dimensional (2D) airflow simulations in an indoor environment and found that FFD can offer much more detailed flow information than do nodal models, with faster-than-real-time simulation speeds. Zuo et al. [12, 13] further improved the accuracy of FFD simulations by using the finite volume method, mass conservation correction, and a hybrid interpolation scheme. Recently, Jin et al. [14, 15, 16] extended FFD to the solution of three-dimensional (3D) airflow and proposed a conservative SL scheme to ensure the conservation of energy and species concentration. Those efforts have made FFD simulations of indoor airflow a viable alternative to CFD simulations, achieving similar accuracy with low computing time and computational capacity.

Nevertheless, there are some limitations associated with using FFD for indoor airflow simulations. The FFD solver developed by Zuo et al. [11] and Jin et al. [14] is applicable only to a hexahedral mesh, which cannot provide a sufficiently accurate depiction of a complex geometry such as the occupants of an indoor space. Therefore, it is essential to develop FFD further for unstructured meshes that can be used to describe complex geometry. This paper reports our effort in implementing FFD in OpenFOAM (Open Field Operation And Manipulation) [17], an open-source CFD program with the capacity to handle a variety of unstructured meshes. To ensure the validity and accuracy of our implementation, this paper also describes the validation of FFD simulation results for different types of indoor airflow with experimental air-distribution data from the literature.

2. Research Method

This section discusses the fundamentals of FFD and describes the implementation of FFD in OpenFOAM.

2.1 Fast fluid dynamics

FFD solves the NS equations in a similar manner to CFD. For incompressible viscous flow in an indoor environment, the NS equations are:

$$\frac{\partial U_i}{\partial x_i} = 0 \tag{1}$$

$$\frac{\partial U_i}{\partial t} + U_j \frac{\partial U_i}{\partial x_j} = -\frac{1}{\rho}\frac{\partial p}{\partial x_i} + \nu \frac{\partial^2 U_i}{\partial x_j \partial x_j} + \frac{1}{\rho} F_i \tag{2}$$

where i, j = 1, 2, and 3. The variable U_i is the i^{th} component of the velocity vector, p pressure, ρ density, F_i the i^{th} component of the body forces, and v kinetic viscosity. FFD applies a three-step time-advancement scheme [18] that splits the momentum equation (Eq. (2)) into three discretized equations (hereafter referred to as the "split scheme"):

$$\frac{U_i^* - U_i^n}{\Delta t} = -U_j^n \frac{\partial U_i^n}{\partial x_j} \tag{3}$$

$$\frac{U_i^{**} - U_i^*}{\Delta t} = \nu \frac{\partial^2 U_i^{**}}{\partial x_j \partial x_j} + \frac{1}{\rho} F_i \tag{4}$$

$$\frac{U_i^{n+1} - U_i^{**}}{\Delta t} = -\frac{1}{\rho}\frac{\partial p}{\partial x_i} \tag{5}$$

where U^n and U^{n+1} represent the velocity at the previous and current time step, respectively. U^* and U^{**} are intermediate velocities. To resolve the coupled pressure and velocity, FFD uses pressure projection [19], which substitutes Eq. (5) into Eq. (1) to produce:

$$\frac{\partial^2 p}{\partial x_i \partial x_i} = \frac{\rho}{\Delta t}\frac{\partial U_i^{**}}{\partial x_i} \tag{6}$$

FFD first solves Eq. (3) with the SL scheme to obtain intermediate velocity U^*. Then FFD solves the two Poisson equations, Eqs. (4) and (6), in sequence to obtain intermediate velocity U^{**} and pressure p, respectively. Finally, FFD calculates the velocity at the next step U^{n+1} by solving Eq. (5). In OpenFOAM, the solution of Eqs. (4), (5), and (6) is straightforward. The following section discusses the use of the SL scheme to solve the advection term, Eq. (3).

2.2 Semi-Lagrangian scheme and implementation in OpenFOAM

The SL scheme applies the Lagrangian advection to a grid so that it will remain stable at large time steps. The scheme traces the flow particle trajectory at each cell back in time to its former position, which is called the departure point, X_d, and copies the quantities at that position to the present cell, which is called the arrival point, X_a. The SL scheme actually solves Eq. (3) by:

$$U^*(X_a) = U^n(X_d) = U^n(X_a - \Delta t U^n(X_a)) \tag{7}$$

where $U^*(X_a)$ is the value of U^* at point X_a, and $U^n(X_d)$ is the value of U^n at point X_d. Since the departure point represents the position of the arrival point in the previous time step, $X_d = X_a - \Delta t U^n(X_a)$. To obtain $U^n(X_d)$, the SL scheme first identifies the index of the departure cell. As illustrated in Figure 1(a), the departure point X_d is not necessarily located at the cell center. Therefore, $U^n(X_d)$ is estimated by interpolation from the values in the surrounding cells, and the result is set as $U^*(X_a)$ in Eq. (7).

For a structured mesh, the cell index can be defined on the basis of the coordinates in the three directions, and thus one can easily find the departure cell. For an unstructured mesh, there is no direct way to define the cell index for the departure point. Giraldo [20] used the QuadTree algorithm to find the closest cell to the departure point for a quadrilateral mesh. This method is fast, but it would fail with a highly distorted mesh and non-convex geometry because the cell closest to the departure point may not be the departure cell. However, Xiu and Karniadakis [21] have presented a fast searching algorithm for the semi-Lagrangian scheme with a 2D mesh. The algorithm can identify the departure cell by checking whether or not the departure point was inside the cells between the arrival and departure points. Figure 1(b) is an example of this process. The search starts with the arrival cell I_a (cell index). To determine whether or not the departure point X_d is inside cell I_a, we can identify the crossover point X_{cr}^a at the cell face f^a by linking X_d and X_a. If point X_d is inside cell I_a and $J = X_d - X_a$, we have

$$J \cdot (X_{cr}^a - X_d) \geq 0 \tag{8}$$

Otherwise, the search moves to the neighboring cell (I_1) of cell face f^a. The same method is applied to determine whether or not the departure point is in cell I_1. If not, the search moves to the next neighboring cell, until

$$J \cdot (X_{cr}^n - X_d) < 0 \tag{9}$$

This result indicates that the departure cell is cell I_n. If cell I_n is outside the flow domain, then the departure cell is considered to be in cell I_{n-1}. The present investigation has extended the concept to three-dimensional meshes. Thus, the index number of the departure cell can be determined.

2.3 Interpolation at the departure cell

Once the index number of the departure cell has been identified, the next step is to obtain $U^n(X_d)$. Since X_d is not necessarily at the cell center, $U^n(X_d)$ is estimated by interpolation from the values in the surrounding cells. To perform the interpolation, this study employed two major interpolation methods, cellPoint and cellPointFace [22], that are embedded in OpenFOAM. The cellPoint method divides each face of the departure cell into triangles, defines a tetrahedron using these triangles and the center-point of the cell, cycles through all the tetrahedrons to determine which one encloses the arbitrary point, and uses inverse distance weights to perform a linear interpolation. In the cellPointFace method, a candidate face is first found by projecting a line from the center of the cell through the arbitrary point; second, the cell face is decomposed into triangles that include the center-point of the face and two vertices; third, these triangles and the cell center-point are used to define a tetrahedron, and the one that encloses the point is identified; and, finally, the inverse distance weights are used to perform a linear interpolation inside the tetrahedron. In both methods, the linear interpolation would induce numerical diffusion, but it can be regarded as a substitute for turbulence viscosity and would be helpful in FFD simulation without turbulence models [14]. Both of the interpolation methods were tested for accuracy.

2.4 Scalar transport equations

For an indoor environment, the transport of energy and species must often be predicted. Therefore, it is also necessary to solve the scalar transport equation:

$$\frac{\partial \Phi}{\partial t} + U_j \frac{\partial \Phi}{\partial x_j} = \Gamma \frac{\partial^2 \Phi}{\partial x_j \partial x_j} + S \tag{10}$$

where Φ is the transport scalar to be solved, Γ the diffusive coefficient, and S the source term. FFD solves the scalar transport equation by the split scheme in the same way as it solves the momentum equations, but without the pressure projection step. FFD splits Eq. (10) into two discretized equations:

$$\frac{\Phi^* - \Phi^n}{\Delta t} = -U_j^n \frac{\partial \Phi^n}{\partial x_j} \tag{11}$$

$$\frac{\Phi^{**} - \Phi^*}{\Delta t} = \Gamma \frac{\partial^2 \Phi^{**}}{\partial x_j \partial x_j} + S \tag{12}$$

Eq. (11) is solved by the SL scheme, and Eq. (12) is solved iteratively. However, a major disadvantage of the SL scheme is that it cannot maintain conservation of the advection quantity

[8]. Jin et al. [16] have proposed a conservative SL scheme that applies a novel mass-fixing method to ensure energy and species conservation. However, the proposed method requires looping over all the grid cells twice, which would not be very efficient if applied in OpenFOAM. Actually, because Eq. (10) is a linear partial differential equation, the time spent on solving it iteratively would not increase the computing cost. Therefore, this investigation proposed an iterative solution of Eq. (10) in FFD, as follows:

$$\frac{\Phi^{n+1}-\Phi^{n}}{\Delta t}+U_j^n\frac{\partial\Phi^{n+1}}{\partial x_j}=\Gamma\frac{\partial^2\Phi^{n+1}}{\partial x_j\partial x_j}+S \tag{13}$$

The implicit scheme was used to ensure stability when the time step size was large. By use of the finite volume method, Eq. (13) could be further discretized to obtain a system of linear equations that could be solved iteratively. Since the temporal term, convection term, diffusion term, and source term for scalar transport have been considered in a single equation, solving Eq. (10) iteratively can ensure the conservation of the scalar Φ.

With the methods proposed here, this study was able to apply the FFD to a structured or unstructured mesh with the cellPoint or cellPointFace interpolation method. It was also possible either to solve the transport equations entirely by the split scheme, or to solve the continuity equation and momentum equations by the split scheme and other scalar transport equation by the iterative scheme (where the combination of the two schemes is hereafter referred to as the "combined scheme"). This investigation tested the accuracy and efficiency of the proposed numerical methods.

3. Results

This study validated the accuracy and applicability of the proposed FFD solver when implemented in OpenFOAM for three indoor airflow cases. Since the study did not incorporate a turbulence model in FFD, we did not intentionally test it with fully developed turbulent flows. The first case was that of isothermal flow in a 2D cavity from Nielsen et al. [23]. This case simulates the airflow in an empty room with forced convection. The two interpolation schemes and two different meshes (structured and unstructured) were tested. The second case was that of non-isothermal flow in a 2D cavity from Blay et al. [24], which was a mixed convection case. The present study solved the energy equation for this case by both the split and iterative methods, and both structured and unstructured meshes were tested. The third case was that of a ventilated three-dimensional room with a heated box from Wang and Chen [25]. The geometry of this case looked simple, but it contained all the flow features encountered in a room: jet, plume, low Reynolds number, and an obstacle. In all three cases, experimental data was available for evaluating the accuracy of the FFD simulations.

3.1 Validation of the FFD solver for forced convection flow in a 2D cavity

The case of forced convection flow in a 2D cavity was from Nielsen et al. [23], who provided detailed experimental data, including the boundary conditions and the air velocity on the four dashed lines shown in Figure 2(a). As the inlet air temperature and wall temperature were identical, it was an isothermal case, and this study did not consider the energy equation.

Figure 2(a) shows the geometry the cavity, where L/H = 3.0, h_{in}/H = 0.056, h_{out}/H = 0.16, and H = 3.0 m. The inlet velocity components were U_1 = 0.455 m/s and U_2 = 0. Figure 2(b) shows the structured mesh (27 × 44) used in the calculations. The grid independence test by Zuo et al. [12] was used as a reference, and therefore this study did not perform a grid independence study. This investigation also generated an unstructured mesh (5960 cells) as shown in Figure 2(c). The grid size of the unstructured mesh was the same as that of the structured mesh.

This study calculated the flow for a physical time of 200 s with a time step size of 1 s. The physical time is long enough to obtain a steady state flow. Using the structured mesh, this study performed calculations with both the cellPoint and cellPointFace interpolation methods. The numerical scheme used was the split scheme. Figure 3 compares the predicted horizontal air velocity U_1 at the x_1 = 2H and x_2 = H - h_{in}/2 sections with the experimental data. It is clear that the calculation with the cellPoint interpolation method is in better agreement with the experimental data. In the following sections, therefore, only the calculations that used the cellPoint interpolation method are presented.

Using this interpolation method, the study validated the FFD solver by applying it to different mesh types. Figures 4(a) and 4(b) show the flow fields predicted by FFD with the split scheme for structured and unstructured meshes. Since the experiment had measured only the air velocity on four lines (the dashed lines in Figure 2(a)), this study used the flow field computed by CFD with the RNG k-ε model [26], as shown in Figure 4(d), as a reference. Because the CFD result agreed very well with the experimental data, as reported by a number of researchers [27, 28], it could be regarded as accurate. The CFD simulation without a turbulence model was also used as a reference because the FFD did not have a turbulence model. The CFD simulations were conducted by using ANSYS Fluent 12.1 [29] with the structured mesh. Figure 4 shows that the FFD solver predicted very similar flow fields with the two different mesh types. FFD predicted one large recirculation pattern and flow separations, as did CFD with the RNG k-ε model. FFD also correctly predicted the jet from the inlet, but it under-predicted the re-circulated flow. The flow fields predicted by FFD agreed qualitatively with that predicted by CFD with the turbulence model. In contrast, the CFD simulation without a turbulence model (laminar flow simulation) had the worst performance because it over-predicted the jet from the inlet and the re-circulated flow.

Figure 5 further compares the horizontal air velocity U_1 predicted by FFD and CFD with the experimental data at x_1 = 2H and x_2 = H - h_{in}/2. The FFD solver predicted similar velocity profiles with different mesh types. Figure 5 again shows that FFD correctly predicted the jet from the inlet, but it did not accurately calculate the re-circulated flow. It is interesting to note that FFD was able to predict the flow recirculation in the upper right corner, but CFD with the RNG k-ε model and the same mesh was not able to. Overall, FFD performed better than CFD without a turbulence model, and the predicted results agreed with the experimental data.

Since the major advantage of FFD compared to CFD is its speed, this study compared the simulation speeds as shown in Table 1. Both FFD and CFD simulations were performed with the aforementioned structured mesh on a personal computer with a single CPU at 3.50 GHz. The FFD simulations were 100 times faster than real-time for the same mesh and time step size. Furthermore, FFD was more than 30 times faster than CFD. The CFD simulation without a turbulence model required a similar computing time to that with the RNG k-ε model because it converged slowly in each time step for the given mesh and time step size.

3.2 Validation of the FFD solver for mixed convection flow in a 2D cavity

This study also tested FFD for the case of mixed convection flow in a 2D cavity from Blay el al. [24]. As shown in Figure 6, the dimensions of the flow domain were W × H = 1.04 m × 1.04 m, the inlet height was h_{in} = 18 mm, and the outlet height was h_{out} = 24 mm. The inlet air velocity components were U_1 = 0.57 m/s and U_2 = 0, and the inlet air temperature (T_{in}) was 15 ºC. The temperature of the two walls and the ceiling (T_w) was 15 ºC, and that of the floor (T_{fl}) was 35 ºC. Therefore, the flow was driven by both inertia and buoyancy. In accordance with the grid independence test by Zuo et al. [12], this study used a 41 × 50 structured mesh and an unstructured mesh with the same grid size (8380 cells). The flow was calculated for a physical time of 100 s. For the structured mesh, a time step size of 0.05 s was used. For the unstructured mesh, because the resolution was finer, a time step size of 0.025 s was used to ensure accuracy.

This study first used FFD with the split scheme to solve the flow and temperature fields with the structured and unstructured meshes. Figures 7(a) and 7(b) show that the two sets of results were quite similar, and FFD performed well with the unstructured mesh. Both simulations predicted one large circulation pattern in the cavity and a secondary recirculation in the upper left corner. The thermal plume caused by the warm floor is also visible. Figure 8 compares the predicted results with the experimental data from Blay el al. [24] in the x/W = 0.5 and y/H = 0.5 sections; the qualitative agreement is good. When the combined scheme was used with the unstructured mesh (Figure 8(d)), the FFD simulations seemed to over-predict the thermal plume generated by the heated floor. A possible reason is that numerical viscosity in FFD enhanced the heat diffusion.

This study then compared the split scheme with the combined scheme for the structured and unstructured meshes in this case. As shown in Figures 7(c) and 7(d), the predicted results with the combined scheme were nearly the same as those obtained with the split scheme. The predicted velocity and temperature profiles with the combined scheme also agreed well with the experimental data (Figure 8). As can be seen in Figure 8(d), the simulations with the combined scheme again over-predicted the thermal plume generated by the heated floor because of the lack of wall-function to treat the thin near-wall sublayer, where viscous effects become important. It is thus hard to accurately predict the near-wall heat transfer. Overall, the combined scheme with the structured mesh seemed to yield slightly better agreement with the experimental data compared with the other methods.

Furthermore, the computing time for the FFD simulations with the structured mesh and the split scheme was 29.58 s, and with combined scheme it was 25.22 s. The combined scheme was more slightly efficient because the split scheme applied the SL scheme to solve the advection term independently, which required extra time to interpolate the air temperature.

3.3 Validation of the FFD solver for mixed convection flow in a 3D room with an obstacle

Finally, this study tested the FFD solver for the case of close-to-realistic flow in a room from Wang and Chen [25]. Figure 9(a) shows a 2.44 m × 2.44 m × 2.44 m room with a plane jet from the upper left corner that developed along the ceiling and reached the far right. The inlet height was 0.03 m. The inlet air velocity was 0.455 m/s with a corresponding Reynolds number of around 2,000, and the supply air temperature was controlled at 22.2 ^{o}C. The flow then moved downwards because of the existence of the right-side wall and formed a circulation pattern in the room. The outlet height was 0.08 m. A heated box in the middle of the room, with dimensions of 1.22 m × 1.22 m × 1.22 m, was used to represent an object such as an occupant or an electric

appliance that would generate a thermal plume. The temperatures of the box surface, ceiling, surrounding walls, and floor were 36.7, 25.8, 27.4, and 26.9 ^{o}C, respectively. Therefore, the type of airflow in the room was mixed convection.

This study used FFD with the split scheme and combined scheme to predict the air velocity and temperature distributions. A CFD simulation with the RNG k-ε model [26] using ANSYS Fluent 12.1 [29] was also performed for this case as a reference. In accordance with the grid independence test by Wang and Chen [25], a structured mesh with 44 × 44 × 44 cells, as shown in Figure 9(b), was used for all the numerical simulations. This study did not consider an unstructured mesh for this case, as the corresponding cell numbers would increase by orders of magnitude if the unstructured mesh had the same grid size as the structured mesh. Since the FFD is designed for fast flow simulation, a coarse grid is always preferred in its application. This study calculated the flow for a physical time of 100 s with a time step size of 0.05 s.

Figure 9(c) shows the 10 positions at which measurements were taken in the experiment. The air velocity and temperature profiles at positions 1, 3, 5, and 6 were selected to validate the predictions because they were in the jet upstream, jet downstream, room center, and a position close to the side wall, respectively. Figure 10 shows the air velocity profiles at the four selected measurement positions, as predicted by FFD with the split scheme, FFD with the combined scheme, and CFD with the RNG k-ε model, and their comparison with the experimental data. It can be seen in the figure that the FFD predictions were similar to those of CFD with the RNG k-ε model. In comparison with the experimental data, FFD with the combined scheme slightly underpredicted the air velocity in some lower part of the room. It may be that the split scheme is very diffusive, which would have added more false turbulence and improved the results.

This case was non-isothermal and Figure 11 compares the predicted temperature profiles with the experimental data in the same positions as in Figure 10. The temperature was normalized by using T_{min} = 22.2 ^{o}C and T_{max} = 36.7 ^{o}C, which were the minimum and maximum temperatures, respectively, that were observed in this case. All the numerical simulations of air temperature agreed well with the experimental data.

4. Discussion

This study tested the FFD solver with structured and unstructured meshes. The predicted results were similar for the two mesh types, with some minor differences. These differences may have been caused by numerical errors, such as truncation and round-off errors. The interpolation procedure in FFD could also contribute numerical errors. To determine whether the differences are significant, this study employed a normalized root mean square error (RMSE) index developed by Wang and Zhai [30]:

$$RMSE(\phi_1,\phi_2)=\frac{3}{r^P-1}\sqrt{\frac{\sum_{k=1}^{m}[\phi_1(k)-\phi_2(k)]^2}{\sum_{k=1}^{N}\phi_2(k)^2}} \tag{14}$$

where ϕ_1 and ϕ_2 are the predicted variables with structured and unstructured meshes, respectively, m is the number of sampled points, r the grid refinement factor, and P the order of the numerical scheme, which was 2 in this investigation. For the 2D cases in this study, we set r as

$$r = \sqrt{\frac{N_{unstructured}}{N_{structured}}} \tag{15}$$

where N is the cell number of the mesh. Table 2 summarizes the mesh resolutions and normalized RMSE results for the 2D cases. Wang and Zhai [30] have proposed that if the normalized RMSE is under 10%, the ϕ_1 and ϕ_2 can be regarded as the same. In the present study, the normalized RMSE for air velocity was larger than 10%, while that for air temperature was less than 10%. Therefore, the difference between the predicted flow fields with structured and unstructured meshes cannot be neglected and a possible reason for the difference is that the non-orthogonality of the unstructured mesh enhanced the numerical diffusion. However, the value of the normalized RMSE for air temperature implies that the difference in the predicted air velocity did not affect the air temperature predictions.

Most of the computing time required for the FFD simulations was used to solve Eq. (3) with the SL scheme (trace-back and interpolation) and the two Poisson equations, Eqs. (4) and (6). In order to verify that the local searching method developed to conduct the trace-back in the SL scheme did not greatly increase the computing time, this study investigated the proportion of the computing time spent on trace-back, interpolation, and solution of the Poisson equations for the room in Section 3.3, as shown in Figure 12. When the time step size was less than or equal to 0.01 s, the proportion of time used for trace-back was as small as 3.6%. This is because the departure point was located in the arrival cell when the time step size was small. The searching method could easily identify the departure cell. As the time step size increased, the proportion of time spent on trace-back also increased because the distance between the departure point and arrival point was proportional to the time step size. However, the trace-back step always required the least computing time.

5. Conclusions

This study implemented FFD in OpenFOAM for applications with structured and unstructured meshes. In order to apply the semi-Lagrangian scheme used in FFD in OpenFOAM, this investigation developed a local searching method to quickly identify the departure cell in an unstructured mesh. The FFD solver in OpenFOAM was then tested by using it to predict the air distribution in a two-dimensional cavity with isothermal flow, in a two-dimensional cavity with mixed convection, and in a three-dimensional room with a heated box. The study led to the following conclusions:

- The cellPoint scheme in OpenFOAM is recommended for conducting the interpolation in the semi-Lagrangian scheme.
- The FFD simulations with the unstructured and unstructured meshes predicted similar air velocity and temperature fields, and both sets of predicted results agreed well with the experimental data.
- FFD simulations with the split scheme for solving the continuity equation and momentum equation and the iterative scheme for solving scalar equation can ensure conservation of the scalars. The computing speed was also slightly faster with this combined scheme than when the split scheme was used to solve all the transport equations, while the results with the two schemes were similar.

Acknowledgement

This material is based upon work supported by the U.S. Department of Homeland Security, Science and Technology Directorate, Office of University Programs, under Grant Award 2013-ST-061-ED0001. The views and conclusions contained in this document are those of the authors and should not be interpreted as necessarily representing the official policies, either expressed or implied, of the U.S. Department of Homeland Security.

References

1. Q. Chen, Ventilation performance prediction for buildings: A method overview and recent applications, *Building and Environment*, vol. 44, no. 4, pp. 848-858, 2009.
2. Q. Chen, K. Lee, S. Mazumdar, S. Poussou, L. Wang, M. Wang, and Z. Zhang, Ventilation performance prediction for buildings: Model assessment, *Building and Environment*, vol. 45, no. 2, pp. 295-303, 2010.
3. L. Wang and Q. Chen, Evaluation of some assumptions used in multizone airflow network models, *Building and Environment*, vol. 43, no. 10, pp. 1671-1677, 2008.
4. A. C. Megri and F. Haghighat, Zonal modeling for simulating indoor environment of buildings: Review, recent developments, and applications, *HVAC&R Research*, vol. 13, no. 6, pp. 887-905, 2007.
5. C. H. Lin, R. H. Horstman, M. F. Ahlers, L. M. Sedgwick, K. H. Dunn, J. L. Topmiller, J. S. Ben-nett, and S. Wirogo, Numerical simulation of airflow and airborne pathogen transport in aircraft cabins–Part I: Numerical simulation of the flow field, *ASHRAE Transactions*, vol. 111, no. 1, pp. 755-763, 2005.
6. T. N. Krishnamurti, Numerical integration of primitive equations by a quasi-Lagrangian advective scheme, *Journal of Applied Meteorology*, vol. 1, no. 4, pp. 508-521, 1962.
7. A. Robert, A stable numerical integration scheme for the primitive meteorological equations, *Atmosphere-Ocean*, vol. 19, no. 1, pp. 35-46, 1981.
8. A. Staniforth and J. Côté, Semi-Lagrangian integration schemes for atmospheric models–A review, *Monthly Weather Review*, vol. 119, no. 9, pp. 2206-2223, 1991.
9. D. Caya and R. Laprise, A semi-implicit semi-Lagrangian regional climate model: The Canadian RCM, *Monthly Weather Review*, vol. 127, no. 3, pp. 341-362, 1999.
10. J. Stam, Stable fluids, *Proceedings of the 26th annual conference on computer graphics and interactive techniques*, ACM Press/Addison-Wesley Publishing Co, 1999.
11. W. Zuo and Q. Chen, Real time or faster-than-real-time simulation of airflow in buildings, *Indoor Air*, vol. 19, no. 1, pp. 33-44, 2009.
12. W. Zuo, J. Hu, and Q. Chen, Improvements on FFD modeling by using different numerical schemes, *Numerical Heat Transfer, Part B: Fundamentals*, vol. 58, no. 1, pp. 1-16, 2010.
13. W. Zuo, M. Jin, and Q. Chen, Reduction of numerical diffusion in the FFD model, *Engineering Applications of Computational Fluid Mechanics*, vol. 6, no. 2, pp. 234-247, 2012.
14. M. Jin, W. Zuo, and Q. Chen, Improvements of fast fluid dynamics for simulating airflow in buildings, *Numerical Heat Transfer, Part B: Fundamentals*, vol. 62, no. 6, pp. 419-438, 2012.

15. M. Jin, W. Zuo, and Q. Chen, Simulating natural ventilation in and around buildings by fast fluid dynamics, *Numerical Heat Transfer, Part A: Applications*, vol. 64, no. 4, pp. 273-289, 2013.
16. M. Jin and Q. Chen, Improvement of fast fluid dynamics with a conservative semi-Lagrangian scheme, *International Journal of Numerical Methods for Heat and Fluid Flow*, vol. 25, no. 1, pp. 2-18, 2015.
17. OpenFOAM, The Open Source CFD Toolbox, http://www.opencfd.co.uk/openfoam.html, 2007.
18. J. H. Ferziger and M. Perić, *Computational Methods for Fluid Dynamics*, Berlin: Springer, vol. 3, pp. 196-200, 2002.
19. A. J. Chorin, A numerical method for solving incompressible viscous flow problems, *Journal of Computational Physics*, vol. 2, no. 1, pp. 12-26, 1967.
20. F. X. Giraldo, The Lagrange-Galerkin spectral element method on unstructured quadrilateral grids, *Journal of Computational Physics*, vol. 147, no. 1, pp. 114-146, 1998.
21. D. Xiu and G. E. Karniadakis, A semi-Lagrangian high-order method for Navier-Stokes equations, *Journal of computational physics*, vol. 172, no. 2, pp. 658-684, 2001.
22. OpenFOAMWiki, OpenFOAM guide/Interpolation (by cell), http://openfoamwiki.net/-index.php/OpenFOAM_guide/Interpolation_(by_cell), 2010.
23. P. V. Nielsen, A. Restivo, and J. H. Whitelaw, The velocity characteristics of ventilated rooms, *Journal of Fluids Engineering*, vol. 100, no. 3, pp. 291-298, 1978.
24. D. Blay, S. Mergui, and C. Niculae, Confined turbulent mixed convection in the presence of a horizontal buoyant wall jet, *Fundamentals of Mixed Convection, ASME HTD*, vol. 213, pp. 65-72, 1992.
25. M. Wang and Q. Chen, Assessment of various turbulence models for transitional flows in enclosed environment, *HVAC&R Research*, vol. 15, no. 6, pp. 1099-1119, 2009.
26. V. Yakhot and S. A. Orszag, Renormalization group analysis of turbulence, *Journal of Scientific Computing*, vol. 1, no. 1, pp. 3-51, 1986.
27. Q. Chen, Comparison of different k-ε models for indoor airflow computations, *Numerical Heat Transfer, Part B: Fundamentals*, vol. 28, pp. 353-369, 1995.
28. W. Zhang and Q. Chen, Large eddy simulation of indoor airflow with a filtered dynamic subgrid scale model, *International Journal of Heat and Mass Transfer*, vol. 43, no. 17, pp. 3219-3231, 2000.
29. ANSYS, ANSYS Fluent 12.1 Documentation, ANSYS, Inc., PA, 2009.
30. H. Wang and Z. Zhai, Analyzing grid independency and numerical viscosity of computational fluid dynamics for indoor environment applications, *Building and Environment*, vol. 52, pp. 107-118, 2012.

Tables

Table 1. Comparison of computing times by FFD with the split scheme and CFD

Physical flow time (s)	Time step size (s)	Elapsed CPU time (s)		
		FFD	CFD without a turbulence model	CFD with the RNG k-ε model
200	1.0	2	67	65

Table 2. Normalized RMSE results for the 2D cases.

Cases	*Solvers*	*Grid number*		*Normalized RMSE*	
		Structured	*Unstructured*	*U*	*T*
Forced convection flow in a 2D cavity	FFD with split scheme	1188	5960	0.1441	N/A
Mixed convection flow in a 2D cavity	FFD with split scheme	2050	8380	0.2126	0.0337
	FFD with combined scheme			0.2091	0.0022

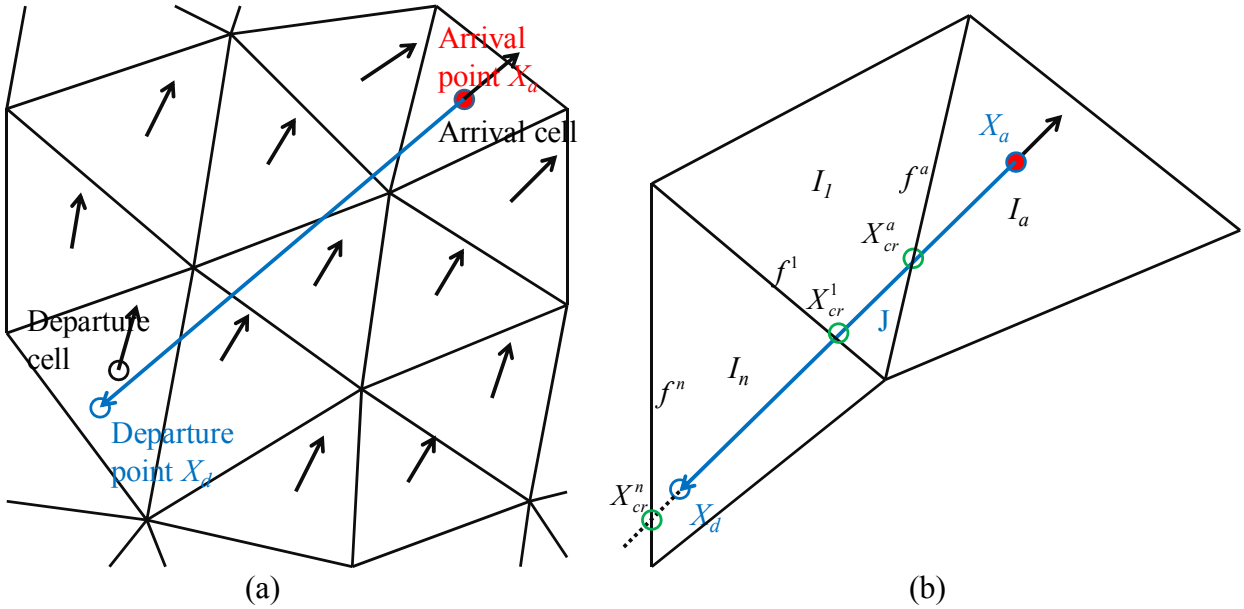

(a) (b)

Figure 1. Illustration of (a) the semi-Lagrangian scheme and (b) the searching algorithm.

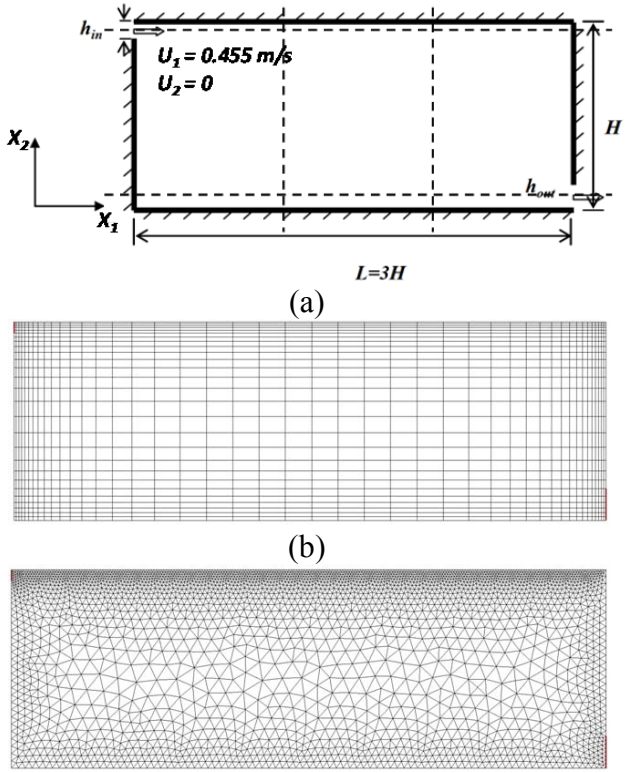

Figure 2. (a) Sketch of the 2D cavity, (b) the structured mesh, and (c) the unstructured mesh used to validate the FFD solver for forced convection flow.

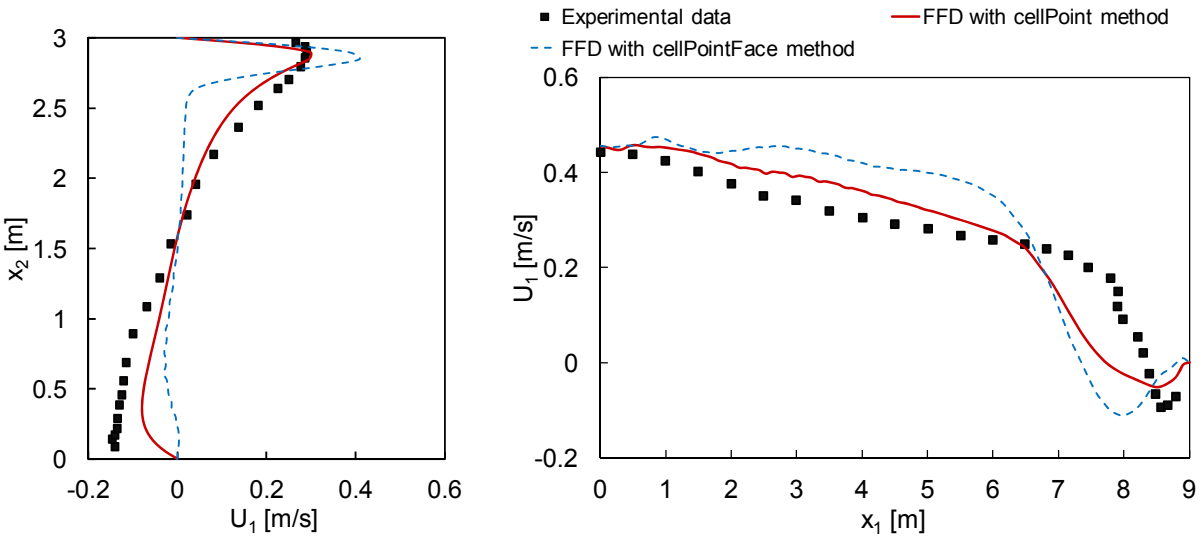

(a) U_1 at $x_1 = 2H$ (b) U_1 at $x_2 = H - h_{in}/2$

Figure 3. Comparison of horizontal air velocity U_1 predicted by FFD using different interpolation methods with the experimental data [23].

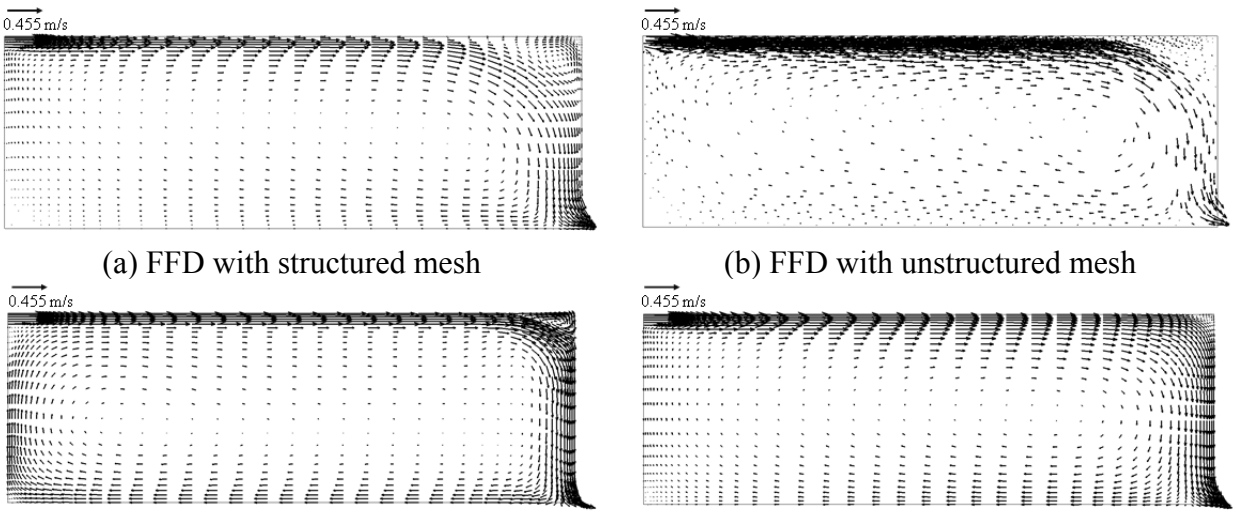

(a) FFD with structured mesh (b) FFD with unstructured mesh

(c) CFD without a turbulence model (d) CFD with the RNG k-ε model

Figure 4. Flow fields predicted by FFD with the split scheme for a structured mesh and unstructured mesh and by CFD without/with the RNG k-ε model for a structured mesh.

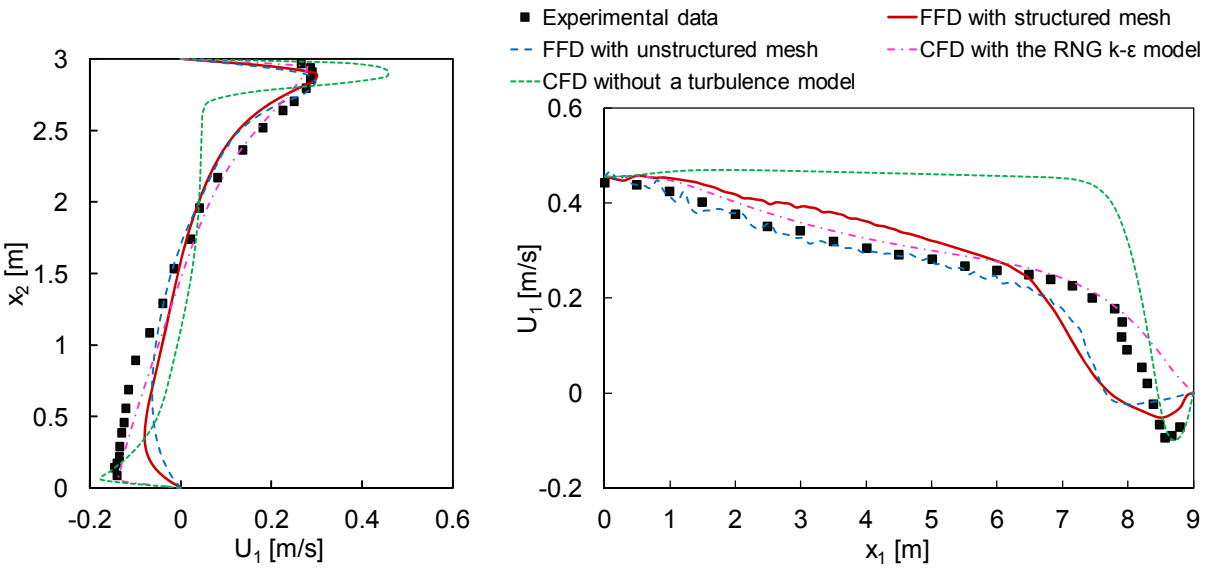

(a) U_1 at $x_1 = 2H$ (b) U_1 at $x_2 = H - h_{in}/2$

Figure 5. Comparison of horizontal air velocity predicted by FFD and CFD with the experimental data [23].

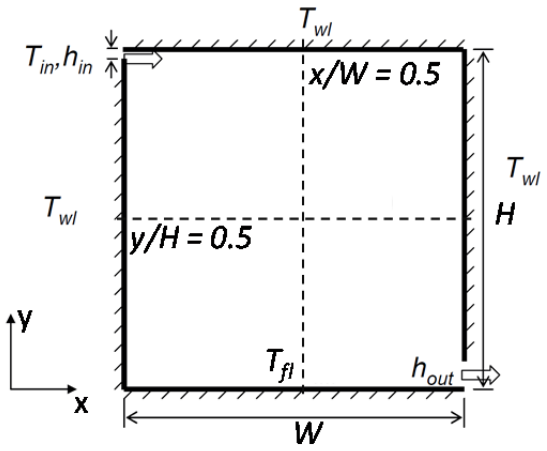

Figure 6. Sketch of the 2D cavity used to validate the FFD solver for mixed convection flow.

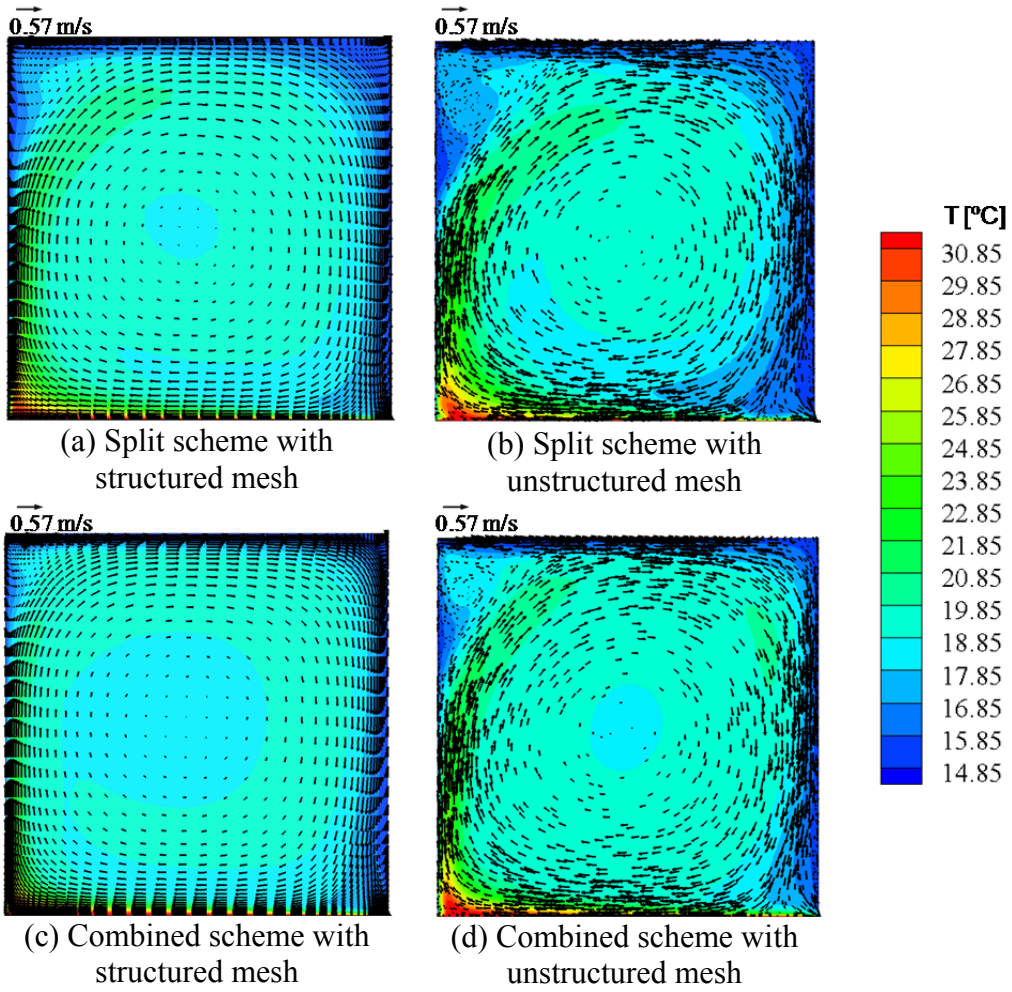

Figure 7. Airflow patterns (arrows) and air temperature fields (color contours) predicted by FFD with different numerical schemes and mesh types

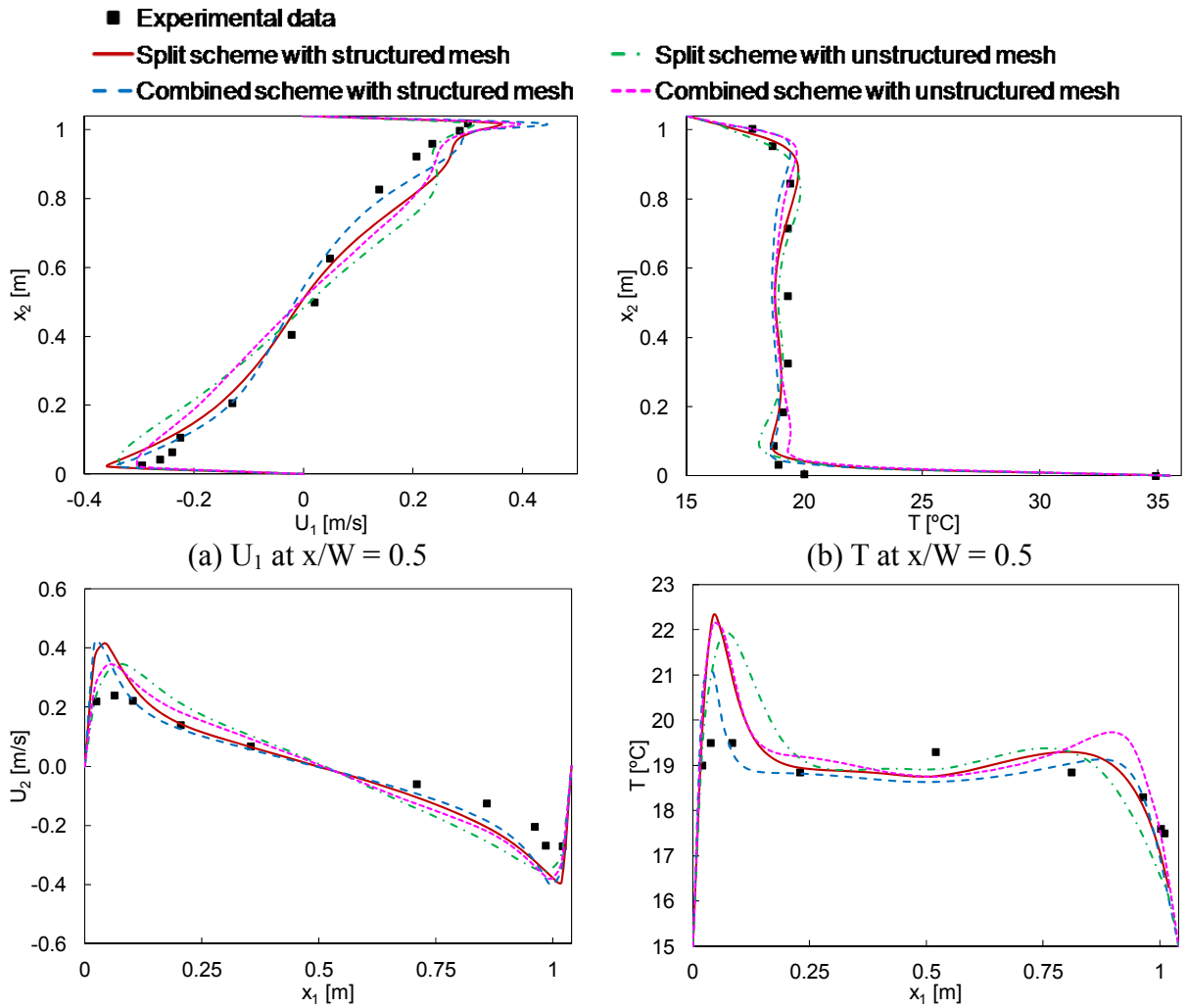

(a) U_1 at x/W = 0.5 (b) T at x/W = 0.5

(c) U_2 at y/H = 0.5 (d) T at y/H = 0.5

Figure 8. Comparison of the air velocity and temperature profiles predicted by FFD with different numerical schemes and mesh types, with the experimental data [24].

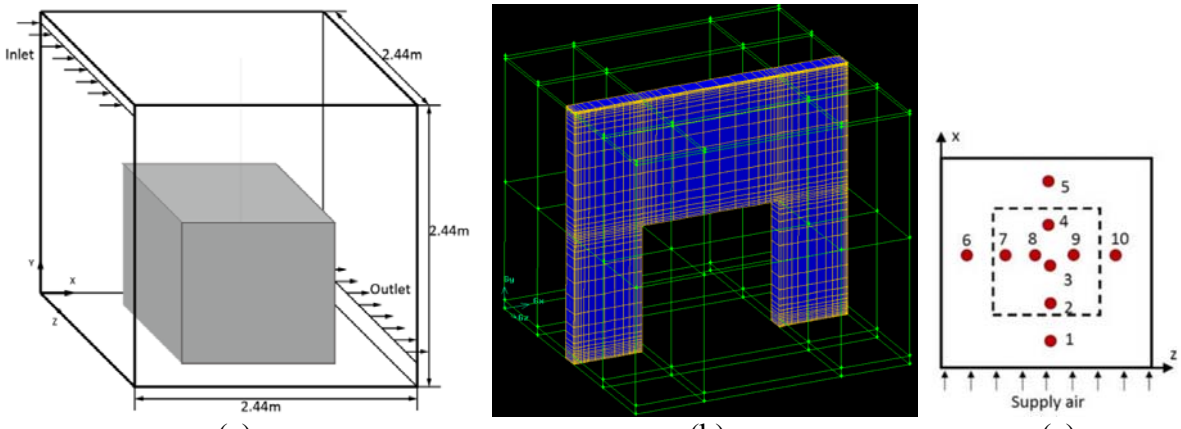

(a) (b) (c)

Figure 9. (a) Sketch of the room with a heated box, (b) the structured mesh, and (c) the measurement positions in the experiment from Wang and Chen [25].

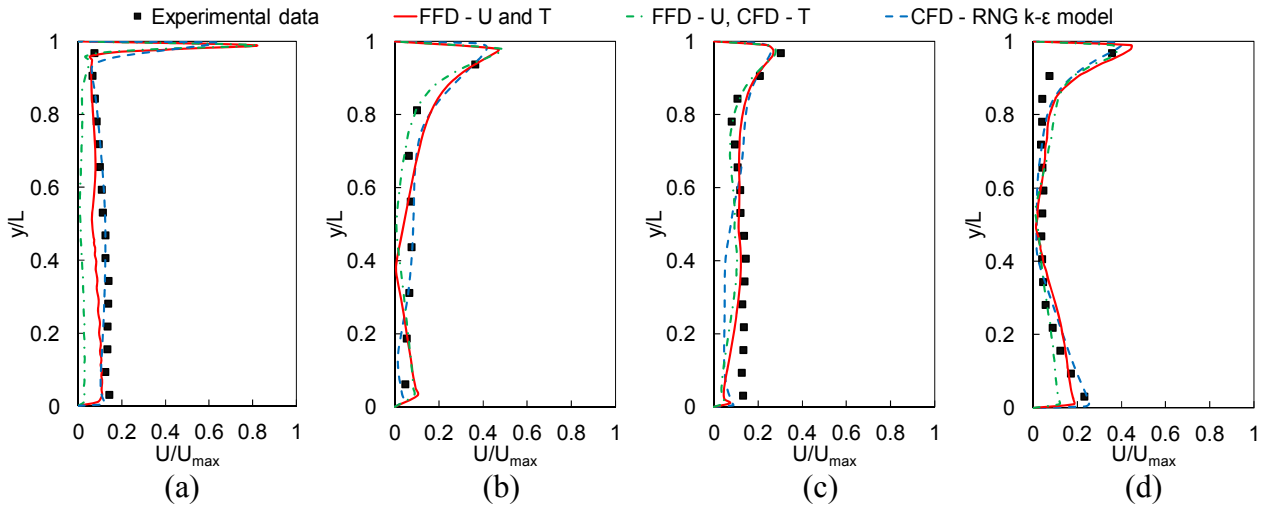

Figure 10. Comparison of air velocity profiles predicted by FFD with the split or combined scheme and by CFD, with the experimental data from Wang and Chen [25] at (a) position 1, (b) position 3, (c) position 5, and (d) position 6.

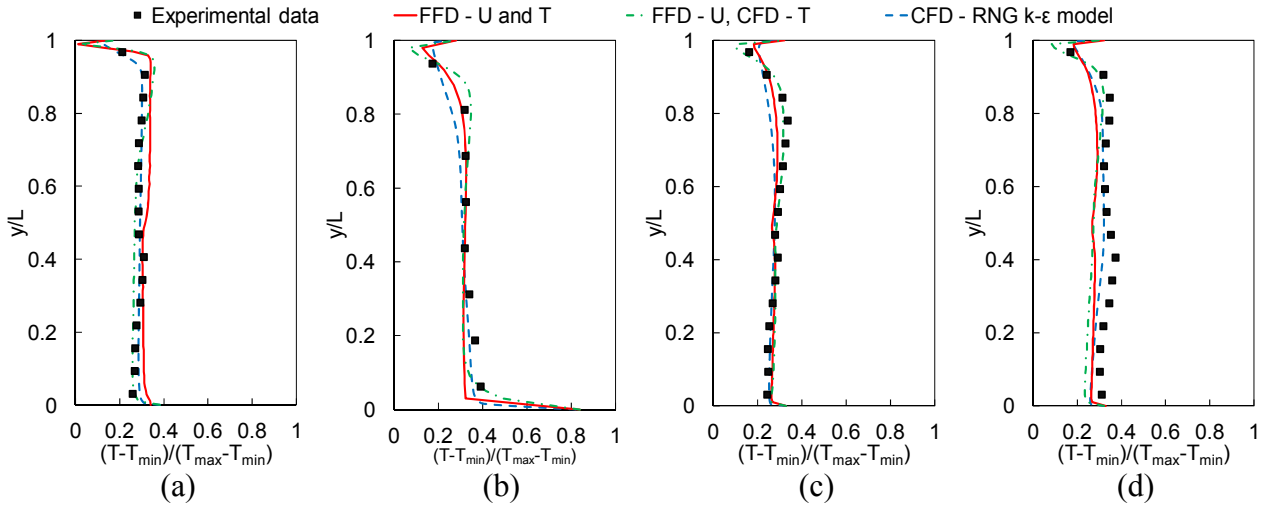

Figure 11. Comparison of air temperature profiles predicted by FFD with the split or combined scheme and by CFD, with the experimental data from Wang and Chen [25] at (a) position 1, (b) position 3, (c) position 5, and (d) position 6.

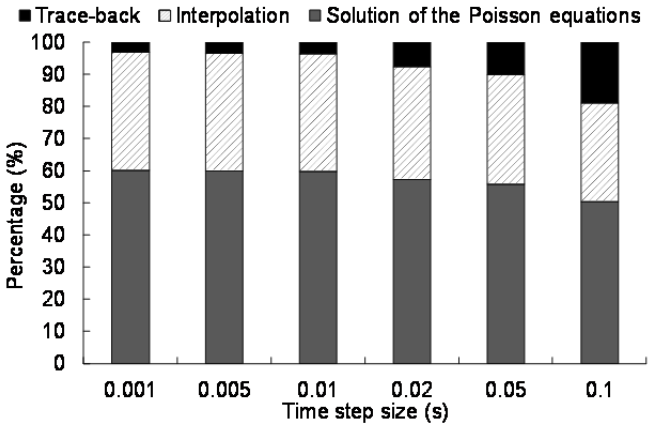

Figure 12. Proportion of computing time on trace-back, interpolation, and solution of the Poisson equations in the room with a heated box.